
Benchmarking Robustness of 3D Point Cloud Recognition Against Common Corruptions

Jiachen Sun¹ Qingzhao Zhang¹ Bhavya Kailkhura² Zhiding Yu³ Chaowei Xiao^{3,4} Z. Morley Mao¹

Abstract

Deep neural networks on 3D point cloud data have been widely used in the real world, especially in safety-critical applications. However, their robustness against corruptions is less studied. In this paper, we present ModelNet40-C, the first comprehensive benchmark on 3D point cloud *corruption robustness*, consisting of 15 common and realistic corruptions. Our evaluation shows a significant gap between the performances on ModelNet40 and ModelNet40-C for state-of-the-art (SOTA) models. To reduce the gap, we propose a simple but effective method by combining PointCutMix-R and TENT after evaluating a wide range of augmentation and test-time adaptation strategies. We identify a number of critical insights for future studies on corruption robustness in point cloud recognition. For instance, we unveil that Transformer-based architectures with proper training recipes achieve the strongest robustness. We hope our in-depth analysis will motivate the development of robust training strategies or architecture designs in the 3D point cloud domain. Our codebase and dataset are included in <https://github.com/jiachens/ModelNet40-C>.

1. Introduction

Point clouds are one of the most acknowledged data format in 3D computer vision tasks, as they are inherently flexible representations and can be retrieved from a variety of sensors and computer-aided design (CAD) models. Because of these strengths, point clouds have been increasingly utilized in real-world applications, particularly in safety-critical areas like self-driving cars (Yin et al., 2021), robotics (Pomerleau et al., 2015), medical imaging (Wang & Solomon, 2019), and virtual and augmented reality (VR/AR) (Maloca et al., 2018). Processing of point clouds is thus crucial un-

der these circumstances. For instance, autonomous vehicles rely on correct recognition of LiDAR point clouds to perceive the surroundings. Similar to 2D image classification, recent efforts demonstrate that deep learning models has dominated the point cloud recognition task.

As opposed to stellar progress on model architectures in 2D computer vision, deep 3D point cloud recognition is emerging where various architectures and operations are being proposed. Classic approaches discretize the point cloud into 3D cells, which causes cubic complexity. PointNet (Qi et al., 2017a) innovates to achieve end-to-end learning on point clouds. A few studies optimize the convolutional operation to be preferable for 3D point cloud learning (Wang et al., 2019; Liu et al., 2019b). Transformer (Vaswani et al., 2017) blocks are also applied as backbones in point cloud recognition architectures (Guo et al., 2021). The most extensively utilized benchmark for comparing methods for point cloud recognition is ModelNet40 (Wu et al., 2015). Although the accuracy on ModelNet40 over the past several years has been steadily improved, it merely shows a single perspective of model performance on the clean data. Given the importance of 3D point cloud in the safety-critical application, a comprehensive *robustness* benchmark for point cloud recognition models is necessary.

In the literature, the vast majority of research on robustness in 3D point cloud recognition has concentrated on the critical difficulties of robustness against adversarial examples. Adversarial training has been adapted to defend against various threats to point cloud learning (Sun et al., 2020b; 2021a). However, we find that the inevitable sensor inaccuracy and physical constraints will result in a number of *common corruption* on point cloud data. For example, occlusion is a typical corruption for LiDAR and other scanning devices, rendering partially visible point clouds. Deformation is also ubiquitous in AR/VR games. Such corruptions pose a even bigger threat in most real-world application scenarios. Therefore, it is imperative to study the corruption robustness of 3D point cloud recognition.

Summary of Our Contributions:

In this paper, we create, to our knowledge, the *first* systematic corruption robustness benchmark, ModelNet40-C, for

¹University of Michigan, Ann Arbor ²Lawrence Livermore National Laboratory ³NVIDIA ⁴ASU. Correspondence to: Jiachen Sun <jiachens@umich.edu>.

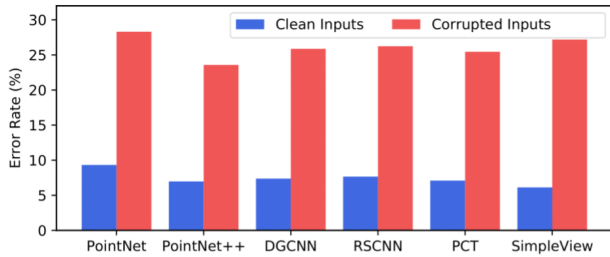


Figure 1. Despite the impressive results on clean inputs (*i.e.*, ModelNet40), state-of-the-art point cloud recognition models cannot deliver good performance on corrupted inputs (*i.e.*, ModelNet40-C). The error rate is $3\times$ larger on ModelNet40-C than ModelNet40.

3D point cloud recognition and present an in-depth analysis. To construct the dataset, we meticulously design and formulate 75 corruptions (15 types with 5 severity levels) that cover the majority of real-world point cloud distortion cases. We further provide a taxonomy of these corruptions into three categories (*i.e.*, density, noise and transformation) and discuss their application scenarios. We anticipate that ModelNet40-C will serve as a first step towards 3D point cloud corruption-resistant models.

We conduct extensive evaluation on our ModelNet40-C. Specifically, we compare six representative models including PointNet (Qi et al., 2017a), PointNet++ (Qi et al., 2017b), DGCNN (Wang et al., 2019), RSCNN (Liu et al., 2019b), PCT (Guo et al., 2021), and SimpleView (Goyal et al., 2021). We find that current models are vulnerable to our created corruptions. As shown in Fig. 1, there are nearly $3\times$ error rate gaps between model performances on ModelNet40 and ModelNet40-C. Our results reveal that ***there is still considerable room for point cloud recognition models to improve on robustness against common corruptions.***

To mitigate such gaps, we propose a simple but effective strategy by combing PointCutMix-R and TENT, after evaluating a wide range of data augmentation and test-time adaptation methods. Our method on average achieves the lowest error rate of 15.4%. Specifically, we try augmentation (or regularization) strategies including PointCutMix-R, PointCutMix-K, PointMixup, RSMix, and adversarial training based strategy. Additionally, we employ test-time adaptation methods (*i.e.*, BN (Schneider et al., 2020) and TENT (Wang et al., 2020)) to show their potential in improving corruption robustness. We examine *every* feasible combinations of architectures and methodologies, a total of 3,180 different configurations of experiments.

We summarize four conclusive insights below and eleven detailed findings in § 5.

- *Insight 1.* Occlusion corruptions, rotation transformation, and background noises pose significant challenges for most point cloud recognition models (§ 5.1).
- *Insight 2.* Different architectures are vulnerable to different corruption types, which can be attributed to their design

principles. (§ 5.2).

- *Insight 3.* Different data augmentation strategies are especially advantageous for certain types of corruptions, which also correlate well with their design choices (§ 5.3).
- *Insight 4.* Test-time adaptations (BN and TENT) are beneficial for enhancing the corruption robustness, particularly for hard corruptions like occlusions and rotations (§ 5.4).

We hope our comprehensive benchmark and in-depth analysis will shed light on the robustness of point cloud recognition, and facilitate the development of robust architectures and training- and test-time robustness strategies on ModelNet40-C.

2. Related Work

Adversarial & Corruption Robustness of 2D Images.

Deep neural networks are known to be vulnerable to adversarial examples and common corruptions (Bulusu et al., 2020). Hendrycks & Dietterich (2019); Hendrycks et al. (2021) developed corruption robustness benchmarking datasets CIFAR-10/100-C, ImageNet-C, and ImageNet-R to facilitate robustness evaluations of CIFAR and ImageNet classification models. Michaelis et al. (2019) extended this benchmark to object detection models. Mintun et al. (2021) further proposed ImageNet-C dataset that is comprised of a set of corruptions that are perceptually dissimilar to ImageNet-C. Recently, Sun et al. (2021b) proposed a comprehensive benchmarking suite CIFAR-10/100-F that contains corruptions from different regions in the spectral domain. (Koh et al., 2021) presented WILDS, a curated benchmark of 10 datasets reflecting a diverse range of distribution shifts that naturally arise in real-world applications. Hendrycks et al. (2019); Cubuk et al. (2018); Calian et al. (2021) proposed augmentation methods to improve the corruption robustness in 2D vision tasks. On the adversarial robustness benchmarking front, Carlini et al. (2019) discussed the methodological foundations, reviewed commonly accepted best practices, and suggested new methods for evaluating defenses to adversarial examples. Croce et al. (2020) proposed a standardized leaderboard called RobustBench, which evaluates the adversarial robustness with AutoAttack (Croce & Hein, 2020), a comprehensive ensemble of white- and black-box attacks.

3D Point Cloud Deep Learning. Deep learning models are increasingly being proposed to process point cloud data. Early works attempted to use 3D voxel grids for perception, which have cubic complexity (Maturana & Scherer, 2015; Wang & Posner, 2015). PointNet (Qi et al., 2017a) pioneered to leverage shared multi-layer perceptrons and a global pooling operation to achieve permutation-invariance and thus enable end-to-end training. Qi et al. (2017b) further proposed PointNet++ to hierarchically stack PointNet for multi-scale local feature encoding. PointCNN and RSCNN

refactor the traditional pyramid CNN to improve the local feature learning for point cloud recognition (Li et al., 2018b; Liu et al., 2019b). The graph data structure is also heavily used in point cloud learning (Landrieu & Simonovsky, 2018; Shen et al., 2018). For example, DGCNN built a dynamic graph of point cloud data for representation learning (Wang et al., 2019). PointConv and KPConv improve the convolution operation for point cloud learning (Wu et al., 2019; Thomas et al., 2019). Recent work demonstrated that ResNet (He et al., 2016) on multi-view 2D projections of point clouds could also achieve high accuracy (Goyal et al., 2021). PointTransformer and PCT advance Transformer (Vaswani et al., 2017) blocks into point cloud learning and achieve state-of-the-art performance (Zhao et al., 2021; Guo et al., 2021).

Robustness Enhancements for 3D Point Cloud. Several recent efforts tackle improving the robustness of 3D point cloud learning (Sun et al., 2020a). Xiang et al. (2019) and Liu et al. (2019a) first demonstrated that point cloud recognition is vulnerable to adversarial attacks. Zhou et al. (2019) and Dong et al. (2020) proposed to leverage input randomization techniques to mitigate such vulnerabilities. Sun et al. (2020b) conducted adaptive attacks on existing defenses and analyzed the application of adversarial training on point cloud recognition. Zhao et al. (2020) discovered that adversarial rotation greatly degrades the perception performance. Sun et al. (2021a) further showed that pre-training on self-supervised tasks enhances the adversarial robustness of point cloud recognition. Recent studies presented a framework that uses the Shapley value (Roth, 1988) to assess the quality of representations learned by different point cloud recognition models (Shen et al., 2021a;b). Recent efforts also proposed certified adversarial defenses (Liu et al., 2021). However, little attention has been paid to the common corruption robustness of point cloud recognition. In this work, we aim to present a systematic benchmark and rigorously analyze the corruption robustness of representative deep point cloud recognition models.

3. 3D Point Cloud Corruption Robustness

In this section, we introduce the design principles of our 3D corruption benchmark. As mentioned in § 1, 3D point clouds are being utilized in various safety- and security-critical real-world applications (Geiger et al., 2012; Adallah et al., 2019; Yu et al., 2021; Cheng et al., 2020). Extensive studies have been carried out to improve both architectures and training strategies for point cloud recognition on in-distribution data (Qi et al., 2017a; Wang et al., 2019; Chen et al., 2020; Lee et al., 2021). However, there has not been any systematic study on the model robustness against common corruption. To bridge this gap, we design 15 common corruptions for benchmarking *corruption robustness* of point cloud recognition models. It is worth

noting that such designs are *non-trivial* since the manipulation space of 3D point clouds is completely different from 2D images where the corruptions come from the RGB modification (Hendrycks & Dietterich, 2019). In particular, we have three principles to design our benchmarks: i) Since we directly manipulate the position of points, we need to take extra care to preserve the *original semantics* of point clouds (Fig. 2). ii) we should ensure the constructed corruptions are *realistic* in various applications. iii) We should take *diversity* as an important factor to emulate a wide range of natural corruptions for 3D point clouds.

Our 15 corruption types can be naturally grouped into three categories (*i.e.*, density, noise, and transformation), and we will introduce them in the following subsections.

3.1. Density Corruption Patterns

3D point cloud can be collected from various sensors like VR scanning devices and LiDAR for autonomous driving, or generated from computer-aided design (CAD) models. Therefore, the testing point clouds may have different density patterns from the training samples. For example, VR scanning (in indoor scenes) and LiDAR sensors may suffer from occlusion, so that only a portion of the point cloud is visible (Geiger et al., 2012; Dai et al., 2017). Besides, the direct reflection of lasers on metal materials will cause local missing points in LiDAR point clouds (Liu et al., 2018). The local density of 3D scanned point clouds rely on how frequently the device passes that area (Nguyen & Le, 2013). We hence formulate five corruption types to cover the density corruption patterns: {Occlusion, LiDAR, Local_Density_Inc, Local_Density_Dec, Cutout}. Specifically, Occlusion and LiDAR both simulate occlusion patterns using ray tracing on the original meshes (Zhou et al., 2018), and LiDAR additionally incorporates the vertically line-styled pattern of LiDAR point clouds (Liu et al., 2018). Local_Density_Inc and Local_Density_Dec will randomly select several local clusters of points using k -nearest neighbors (k NN) to increase and decrease their density, respectively. Similarly, Cutout discards several randomly chosen local clusters of points using k NN (DeVries & Taylor, 2017).

3.2. Noise Corruption Patterns

Noise evidently exists in all real-world point cloud applications. For example, the inevitable digital noise of scanning sensors (*e.g.*, medical imaging) (Wolff et al., 2016) and the random reflections and inaccuracy of LiDAR lasers (Geiger et al., 2012) will contribute to a substantial variation of points. Compression and decompression will potentially result in noisy point clouds as well (Cao et al., 2019). Besides, real-time rendering in VR games is another source of noise (Bonatto et al., 2016). Although noise is a common corruption pattern for both 2D and 3D data, the manip-

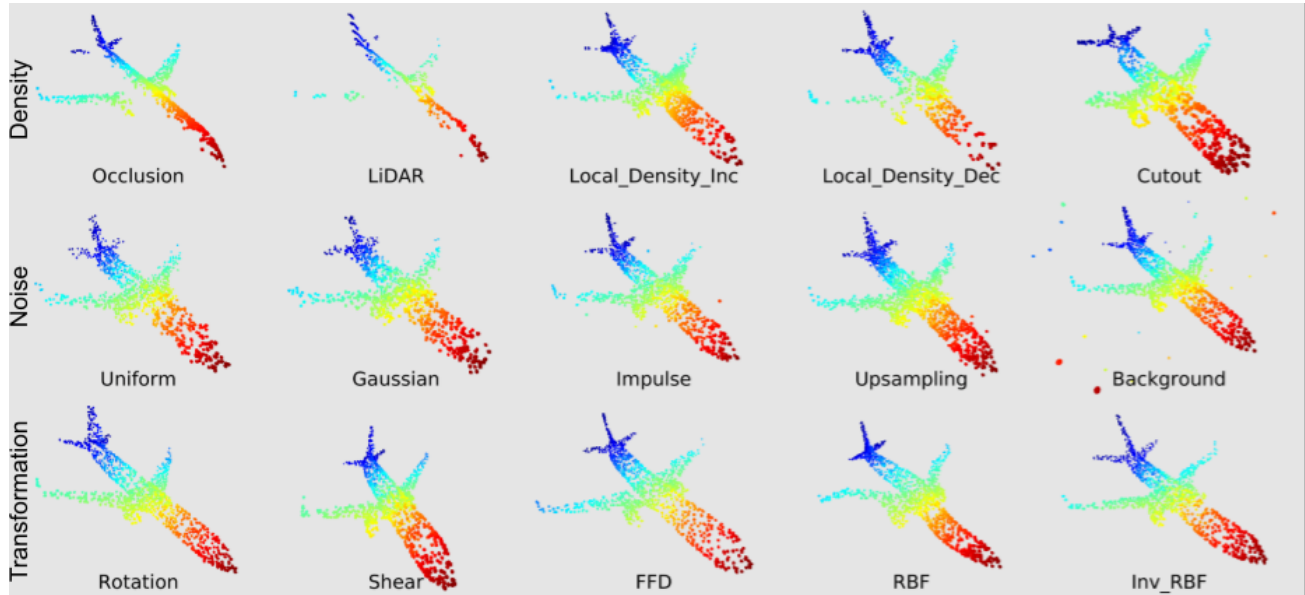


Figure 2. Visualizations of Our Constructed ModelNet40-C. Our ModelNet40-C dataset consists of 15 corruption types that represent different out-of-distribution shifts in real-world applications of point clouds. Similar to ImageNet-C (Hendrycks & Dietterich, 2019), each corruption type has five severity levels. We carefully examine the generated point clouds and ensure they preserve their original semantics. More visualization samples are shown in Appendix A

ulation space is larger for point clouds since their numbers of points are adjustable. We thus formulate five noise perturbations: {Uniform, Gaussian, Impulse, Upsampling, Background}. As their names indicate, Uniform and Gaussian apply different distributional noise to each point in a point cloud. Impulse applies deterministic perturbations to a subset of points. Upsampling assigns new perturbation points around the existing points. Background randomly adds new points in the bounding box space of the pristine point cloud.

3.3. Transformation Corruptions Patterns

We use both linear and non-linear 3D transformations to formulate the corruptions. For the linear ones, we leverage 3D Rotation and Shear as our corruption types and exclude translation and scale transformations since they can be easily restored by normalization (*i.e.*, the inverse transformation matrix). Rotation of point clouds is common in the real world and the robustness against adversarial rotations has been investigated by a few studies (Zhao et al., 2020; Shen et al., 2021a). We here do not use aggressive rotations that might affect human perception as well, but instead enable a milder rotation ($\leq 15^\circ$) along xyz axes. We consider Shear on the xy plane to represent the motion distortion in 3D point clouds (Yang et al., 2021). We utilize free-form deformation (FFD) (Sederberg & Parry, 1986) and radial basis function (RBF)-based deformation (Forti & Rozza, 2014) for non-linear transformations. Such deformations are also common in VR/AR games and point clouds from generative models (GAN) (Li et al., 2018a;

Zhou et al., 2021). Specifically, we use multi quadratic ($\varphi(\mathbf{x}) = \sqrt{\mathbf{x}^2 + r^2}$) and inverse multi quadratic splines ($\varphi(\mathbf{x}) = (\mathbf{x}^2 + r^2)^{-\frac{1}{2}}$) as the representative RBFs to cover a wide range of deformation types. As a result, we in total formulate {Rotation, Shear, FFD, RBF, Inv_RBF} as our transformation-based corruptions.

4. ModelNet40-C Robustness Benchmark

ModelNet40 is the most popular dataset for benchmarking point cloud recognition performance, containing 12,308 point clouds from 40 classes (Wu et al., 2015). Point clouds from ModelNet40 are extracted from CAD models, rendering a perfectly clean dataset. Uy et al. (2019) recently proposed ScanObjectNN consisting of point clouds scanned from real-world objects to show the performance gap between models trained on synthetic and real-world data. However, quantifying how models trained on the clean dataset perform under common corruptions encountered during the test time remains challenging. To this end, we use the ModelNet40 as our base dataset to construct ModelNet40-C. It is worth noting that our devised corruptions are general to be applied to other dataset, like ShapeNet (Chang et al., 2015).

Setup. We create ModelNet40-C with five severity levels for each corruption type, the same as ImageNet-C. Fig. 2 illustrates samples from ModelNet40-C with severity level four, and they clearly still preserve the semantics of the “air-plane” class. Since it is hard to qualify and quantify the corruption severity for LiDAR and Occlusion, we instead leverage five different view angles to create their corrupted point clouds. The detailed construction of ModelNet40-C

Table 1. Error Rates of Different Models with Training Strategies on the ModelNet40 (ER_{clean}). **Bold** and underline denote the best and runner-up results throughout this paper, respectively.

Model (%) ↓	Standard	PointCutMix-R	PointCutMix-K	PointMixup	RSMix	PGD
PointNet	9.3	9.4	9.0	8.9	9.8	11.8
PointNet++	<u>7.0</u>	7.1	6.7	7.1	6.6	-
DGCNN	7.4	7.4	6.8	7.8	7.1	8.1
RSCNN	7.7	7.6	7.1	<u>7.2</u>	7.6	-
PCT	7.1	<u>7.2</u>	6.9	7.4	6.9	<u>8.9</u>
SimpleView	6.1	7.9	7.4	<u>7.2</u>	7.9	-

is introduced in Appendix A. These designed corruptions are applied to the *validation* set of ModelNet40, resulting in ModelNet40-C a $75\times$ larger dataset to test the corruption robustness of pre-existing models. *Note that ModelNet40-C should be only used in the test time rather than in the training phase.*

Metrics. We use the error rate (ER) and class-wise mean error rate (mER) as the main metrics for ModelNet40-C benchmarking. We denote ER_{clean}^f as the error rate for a classifier f on the clean dataset (*i.e.*, ModelNet40) and $ER_{s,c}^f$ as the error rate for f on corruption c with severity s . Similarly, $ER_c^f = \sum_{s=1}^5 ER_{s,c}^f$ and $ER_{\text{cor}}^f = \sum_{c=1}^{15} ER_c^f$. We will release our leaderboard publicly to facilitate future studies on robustness of point cloud learning. The goal of ModelNet40-C is to evaluate the general robustness of point cloud learning models in various real-world scenarios. ModelNet40-C is not designed for training-time optimizations but augmentations with other/similar corruptions are allowed and should be explicitly stated. The corruption robustness of trained models can be assessed by their performance on ModelNet40-C using above metrics.

5. Experiments

In this section, we elaborate our comprehensive evaluation and rigorous analysis in detail. We benchmark corruption robustness of point cloud recognition from the perspectives of corruption types and model architectures. Moreover, we examine the effectiveness of data augmentations and test-time adaptation methods as mitigation solutions against common corruptions.

Setup. We leverage six representative model architectures: PointNet (Qi et al., 2017a), PointNet++ (Qi et al., 2017a), DGCNN (Wang et al., 2019), RSCNN (Liu et al., 2019b), PCT (Guo et al., 2021), and SimpleView (Goyal et al., 2021). These six models stand for distinct architecture designs, and have achieved good accuracy on the clean dataset. They are also well-recognized by the 3D vision community, and have been extensively applied to complex tasks like semantic segmentation (Nguyen & Le, 2013) and object detection (Shi et al., 2019; 2020). As suggested by Goyal et al. (2021), we adopt the same training strategy for all models. We utilize smoothed cross-entropy (Wang et al., 2019) as the loss function as it has been demonstrated to improve the recognition performance. We take 1024 points as input size in the train-

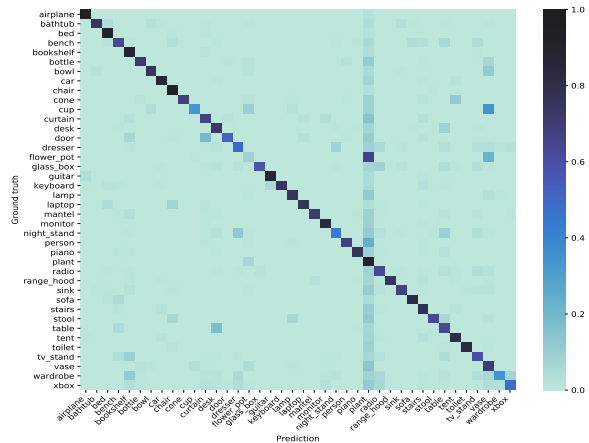


Figure 3. Confusion Matrix on ModelNet40-C Averaged over Six Models with Standard Training. Confusion matrices for each model are shown in Figure 8 in Appendix B.

ing phase and use the Adam optimizer (Kingma & Ba, 2014) with the ReduceLRonPlateau scheduler implemented in PyTorch (Paszke et al., 2019). We train 300 epochs and pick the best performant model for our further evaluation and follow Wang et al. (2019) to use random translation and scaling as our default data augmentation. All training and testing experiments are done on a GeForce RTX 2080 GPU. We report the class-wise mean ER in Appendix B due to space constraints.

Besides, we try data augmentation and test-time adaption strategies and evaluate their effectiveness against our created corruptions. In particular, we leverage PointCutMix-R, PointCutMix-K (Zhang et al., 2021), PointMixup (Chen et al., 2020), RSMix (Lee et al., 2021), and PGD-based adversarial training (Sun et al., 2021a) as additional data augmentation strategies. We adopt the original hyper-parameter settings from their official implementations in our study. Detailed introduction can be found in Appendix B. We only enable adversarial training for PointNet, DGCNN, and PCT since PointNet++ and RSCNN leverage ball queries to find neighboring points and SimpleView projects the pristine point cloud into multi-view 2D images. Both methods will hinder the gradients from backward propagating to the original point cloud, making adversarial training inapplicable. We leave them as future work.

Clean Performance. Table 1 shows the ER_{clean} of different model architectures with the adopted training strategies. All models achieve 90+% accuracy with standard training. As Goyal et al. (2021) indicate, auxiliary factors will obscure the effect of architectures, and the performance gaps among different models are not significant on the ModelNet40 validation set. Data augmentation strategies like PointMixup claim to enhance the general model performance. However, with these factors controlled, we also do not find tangible improvements over these augmentation recipes. Besides, adversarially trained models are expected

Table 2. Error Rates of Different Model Architectures on ModelNet40-C with Standard Training.

Model (%) ↓	ER _{cor}	Density Corruptions					Noise Corruptions					Transformation Corruptions				
		Occlusion	LiDAR	Density Inc.	Density Dec.	Cutout	Uniform	Gaussian	Impulse	Upsampling	Background	Rotation	Shear	FFD	RBF	Inv. RBF
PointNet	28.3	<u>52.3</u>	54.9	10.5	<u>11.6</u>	<u>12.0</u>	<u>12.4</u>	14.4	29.1	14.0	93.6	36.8	25.4	21.3	18.6	17.8
PointNet++	23.6	54.7	<u>66.5</u>	16.0	10.0	10.7	20.4	16.4	35.1	<u>17.2</u>	<u>18.6</u>	27.6	13.4	15.2	16.4	15.4
DGCNN	25.9	59.2	81.0	14.1	17.3	15.4	14.6	16.6	<u>24.9</u>	19.1	53.1	<u>19.1</u>	<u>12.1</u>	<u>13.1</u>	<u>14.5</u>	<u>14.0</u>
RSCNN	26.2	51.8	68.4	16.8	13.2	13.8	24.6	18.3	46.2	20.1	18.3	29.2	17.0	18.1	19.2	18.6
PCT	<u>25.5</u>	56.6	76.7	<u>11.8</u>	14.3	14.5	12.1	13.9	39.1	17.4	57.9	18.1	11.5	12.4	13.0	12.6
SimpleView	27.2	55.5	82.2	13.7	17.2	20.1	14.5	<u>14.2</u>	24.6	17.7	46.8	30.7	18.5	17.0	17.9	17.2
Average	26.1	55.0	71.6	13.8	13.9	14.4	16.4	15.6	33.2	17.6	48.0	26.9	16.3	16.2	16.6	15.9

to perform slightly worse on the clean dataset compared to others (Sun et al., 2021a). It also initiates that model performances on ModelNet40 tend to saturate. Thus, it is a necessary to evaluate the model effectiveness from other perspectives (e.g., robustness).

5.1. Comparison Among Corruption Types

Validity. We first benchmark robustness of six standard trained models to verify the validity of our ModelNet40-C. The detailed results are presented in Fig. 9 and 10 in Appendix B. We find that the ER_{s,c} gradually increases as the severity level increasing for each corruption, which justifies our hyper-parameter setting. As shown in Fig. 1, there is a $\sim 3\times$ performance degradation between the overall ER_{cor} and ER_{clean} for all benchmarked models. Fig. 3 shows the average confusion matrix over six models and 15 corruptions, where the values in the diagonal are still high, further validating the semantic maintenance of ModelNet40-C. ModelNet40-C fullfills its goal as a robustness benchmark for future studies.

Table 2 presents the detailed ER_c of the six models evaluated on ModelNet40-C with standard training. As mentioned before, there is a significant increase in ER_c on each corruption compared to ER_{clean}. The gap ranges from 17.6% to 89.7% among different corruptions. From the perspective of the corruption, we obtain several interesting observations.

- *Insight 1.1.* Occlusion and LiDAR corruptions pose a major threat for 3D point cloud recognition models.

From Table 2, ER_{Occlusion} and ER_{LiDAR} reach 55.0% and 71.6% on average, respectively. Occlusion happens in most real-world application of 3D point clouds. Moreover, we find the models have poor performance regardless of the occlusion directions, suggesting a general vulnerability of point cloud recognition.

- *Insight 1.2.* Rotation is still a challenging corruption for 3D point cloud recognition models even with small angles.

Rotation is a well-known threat for point cloud recognition by several recent studies (Zhao et al., 2020; Shen et al., 2021a). Existing studies allow a rotation angle (e.g., $\geq 45^\circ$). However, such rotated point clouds confuse human perception without RGB information. In our study, we find that a small rotation ($\leq 15^\circ$) still causes a high ER on point

cloud recognition models ranging from 18.1% to 36.8%.

- *Insight 1.3.* Impulse and Background corruptions are surprisingly troublesome to 3D point cloud recognition.

We find ER_{Impulse} (33.2%) and ER_{Background} (48.0%) are abnormally high for most architectures. Although they are even less perceptible than Gaussian and uniform noise since only a small portion of points are affected. However, the magnitudes of Impulse and Background noises are high, suggesting that a small portion of outliers will greatly affect point cloud recognition performance.

5.2. Comparison Among Model Architectures

As presented in Table 2, there is no overarching model that dominates our ModelNet40-C dataset, unlike robustness benchmarking in 2D vision (Hendrycks & Dietterich, 2019). Point cloud recognition models have various designs and no consensus has been reached as deep learning in the 3D space is a relatively nascent field. The model performances on ModelNet40-C are found to be in good alignment with their design attributes.

- *Insight 2.1.* PointNet achieves strong performance on density corruptions, but fails on transformation corruptions.

PointNet does not encode local feature, and several publications have studied it from the perspectives of adversarial robustness (Sun et al., 2021a) and representation quality (Shen et al., 2021a). Such a design has been regarded as a main drawback of PointNet. However, we find it robust against the variations in density. Table 2 presents that PointNet achieves an ER of 28.3% on density corruptions, and overall outperforms the runner-up by 11.7%. Such results can be attributed to the locality of density corruptions. Compared to other models that embeds complex local features, PointNet is less sensitive to local changes of the input point cloud. On the other hand, PointNet indeed fails on other corruptions, rendering itself the worst performant model on average. Our analysis complements the existing understanding of PointNet, we believe the usage of PointNet should be determined by the application scenarios.

- *Insight 2.2.* Ball query-based clustering operation is robust against Background noise.

As mentioned in § 5.1, Background is a challenging corruption to point cloud recognition. However, we find that

Table 3. Error Rates of Different Model Architectures on ModelNet40-C with Different Data Augmentation Strategies.

Model (%) ↓	Standard		PointCutMix-R			PointCutMix-K			PointMixup			RSMix			PGD						
	ER _{cor}	ER _{cor}	Density	Noise	Trans.	ER _{cor}	Density	Noise	Trans.	ER _{cor}	Density	Noise	Trans.	ER _{cor}	Density	Noise	Trans.	ER _{cor}	Density	Noise	Trans.
PointNet	28.3	21.8	30.5	18.0	16.9	21.3	26.8	21.8	15.4	25.4	28.3	28.9	19.0	22.5	24.8	27.3	15.5	25.9	28.8	28.4	20.5
PointNet++	23.6	19.1	28.1	12.2	17.0	20.2	<u>26.3</u>	16.9	17.3	19.3	30.8	14.3	12.9	23.3	27.0	19.3	23.7	-	-	-	-
DGCNN	25.9	<u>17.3</u>	28.9	11.4	<u>11.5</u>	<u>17.3</u>	29.1	11.9	10.9	20.4	32.1	16.8	<u>12.3</u>	<u>18.1</u>	28.8	<u>13.0</u>	12.6	<u>20.7</u>	36.8	13.8	<u>11.5</u>
RSCNN	26.2	17.9	25.0	13.0	15.8	21.6	28.3	19.0	17.6	19.8	<u>29.7</u>	<u>15.5</u>	14.1	21.2	26.8	17.4	19.3	-	-	-	-
PCT	<u>25.5</u>	16.3	<u>27.1</u>	10.5	11.2	16.5	25.8	<u>12.6</u>	<u>11.1</u>	<u>19.5</u>	30.3	16.7	11.5	17.3	25.0	12.0	<u>15.0</u>	18.4	<u>29.3</u>	<u>14.7</u>	11.1
SimpleView	27.2	19.7	31.2	<u>11.3</u>	16.5	20.6	29.1	15.6	17.0	21.5	32.7	17.1	14.8	20.4	28.4	14.6	18.3	-	-	-	-
Average	26.1	18.7	28.5	12.7	14.8	19.6	27.6	16.3	14.9	21.0	30.6	18.2	14.1	20.5	26.8	17.3	17.4	-	-	-	-

PointNet++ and RSCNN are specially robust against it, which have outperform other models by 70.7%. We discover that the ball query of neighboring points is the key to such robustness. Compared to k NN that has deterministic k points to cluster, ball query fixes the radius to reject faraway points in the bounding box space. This design helps models tackle the root cause of the Background corruption.

• *Insight 2.3.* Transformer-based architectures are robust against transformation corruptions.

Transformer (Vaswani et al., 2017) has recently reformed the 2D vision (Dosovitskiy et al., 2021). PCT leverages multiple Transformer blocks as its backbone, which leverage self-attention modules to embed robust global features. PCT reaches the ER of 13.5% on transformation corruptions, consistently achieving the best model on all corruption types. In comparison to density and noise corruptions, transformation corruptions are mild and have a minor effect on the local smoothness. Transformer has been demonstrated to have large capacity and a global receptive field, and we believe this design contribute to its resilience to global corruption of point clouds.

Besides above, we find that SimpleView cannot achieve better robustness under common corruptions than other architectures, despite it high performance on clean data (Table 2), suggesting point cloud-specific designs are indeed desired. Due to its good results on Background, PointNet++ on average performs the best with standard training, achieving an ER_{cor} of 23.6%, and PCT has a more balanced performance across corruptions, making it the runner-up architecture.

5.3. Data Augmentation Strategies

As mentioned earlier, we use five additional data augmentation strategies to train the six models. In this section, we examine how these training recipes combined with different models perform on ModelNet40-C, and Table 3 presents the overall results. Due to the space limit, we group the evaluation results per corruption patterns and the detailed results are shown in Fig. 9 and 10 in Appendix B. Several interesting insights can be concluded from our experiments.

• *Insight 3.1* Data augmentation strategies generally improve the corruption robustness of 3D point cloud recognition.

As Table 3 indicates, all the augmentation recipes enhance

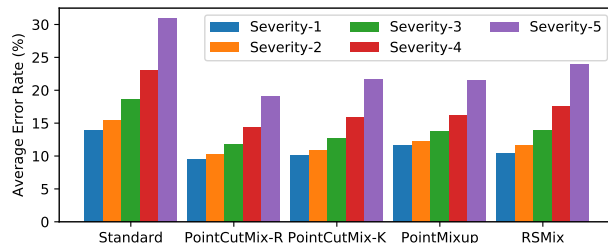


Figure 4. Average Error Rates over Six Models and 13 Corruptions (except for Occlusion and LiDAR). We exclude Occlusion and LiDAR since they do not have different severity levels.

the overall corruption robustness from 19.6% to 28.4%. Data augmentation methods enrich the training set the resulting model more general. Combined with results in Table 1, our paper suggests different conclusions from the original claims: mixing-based augmentations have little gain on clean performance but help generalize to common corruptions.

• *Insight 3.2.* No single data augmentation can rule them all. Different augmentation methods have expertise on distinct corruption patterns.

As Table 3 presents, PointCutMix-R performs the best on noise corruptions (ER = 12.7%), PointMixup specializes the transformation corruptions (ER = 14.1%), and RSMix is especially robust against density corruptions (ER = 26.8%). Such results also relate to the design of augmentation strategies. In details, given two point cloud samples x_a, x_b from class a and b , PointCutMix-R simply merges (\oplus) two randomly selected (\odot) subsets together based on hyper-parameter λ ($x_{aug} = \lambda \odot x_a \oplus (1 - \lambda) \odot x_b$). The two subsets will overlap in the resulting point cloud x_{aug} . Each point cloud subset can be regarded as a special noise by the other. Thus, it naturally includes noise corruptions with mixing into data augmentations. PointMixup leverages interpolation-based mixing that the transition between two point clouds ($x_{aug} = \lambda x_a + (1 - \lambda) \zeta(x_a, x_b)$, where $\zeta(x_a, x_b)$ finds the shortest path for every pair in x_a and x_b). The augmented point cloud is thus locally smooth, which aligns with the transformation corruptions. In contrast, RSMix acts similarly with PointCutMix-K but guarantee a *rigid* mixing of two partial point clouds. There will be no overlaps and each point cloud subset is clustered and isolated in the 3D space. Such patterns correspond to density corruptions in point cloud data.

Table 4. Error Rates of Different Model Architectures on ModelNet40-C with Different Test-time Adaptation Methods.

Model (%) ↓	BN				TENT			
	ER _{cor}	Density	Noise	Trans.	ER _{cor}	Density	Noise	Trans.
PointNet	25.9	26.8	29.6	21.2	27.3	27.8	31.0	23.0
PointNet++	16.9	24.2	12.7	13.8	16.7	24.1	<u>12.3</u>	13.6
DGCNN	21.1	31.4	19.5	<u>12.5</u>	20.9	30.7	19.4	<u>12.5</u>
RSCNN	20.0	26.4	16.7	17.0	19.4	26.0	15.9	16.4
PCT	<u>19.5</u>	27.9	18.2	12.4	18.0	<u>26.9</u>	15.4	11.7
SimpleView	19.8	29.8	<u>13.8</u>	15.8	<u>16.9</u>	28.1	9.9	12.8
Average	20.5	27.7	18.4	15.4	19.9	27.3	17.3	15.0

• *Insight 3.3.* Adversarial training does not show superiority on corruption robustness for 3D point cloud recognition.

Adversarial training improves robustness on noise corruptions since we rely on point shifting attacks in the inner maximization stage. Shen et al. (2021a) suggest that adversarial rotation training improves the robustness against random rotations. We here motivate future research to present general methods that improve both adversarial and corruption robustness for point cloud learning.

Moreover, with more data augmentation and we find PCT outperforms PointNet++ with augmentation sophisticated training recipes. Such results align with recent studies in corruption robustness of 2D vision tasks as well (Bai et al., 2021), suggesting the superiority of Transformer-based design in 3D point cloud learning. Surprisingly, the simplest augmentation, PointCutMix-R, achieves the best overall robustness (ER_{corrupt}=18.7%). As Fig. 4 shows, it is especially helpful on corruptions with high severity levels. We hope our analysis will facilitate future research on designing effective and robust training recipes.

5.4. Test-Time Adaptation Methods

Besides the introduced training-time strategies, we evaluate test-time adaptation methods on our ModelNet40-C. Specifically, we for the first time adapt the BN (Schneider et al., 2020) and TENT (Wang et al., 2020) to point cloud recognition. BN updates the statistics of BatchNorm (Ioffe & Szegedy, 2015) layers (*i.e.*, μ and σ .) based on the incoming batch of testing point clouds. TENT updates both the statistics and weight parameters (*i.e.*, γ and β .) of BatchNorm layers to minimize the cross-entropy of the output layer. Table 4 presents the evaluation results.

• *Insight 4.1.* Test-time adaptations overall perform worse than data augmentation strategies in improving robustness.

BN and TENT consistently help enhance the corruption robustness for point cloud recognition. However, we find they overall are not as effective as data augmentation strategies. Such observations are different from 2D vision tasks, and we attribute the reason to the nature of corruptions in 3D space. Corruption robustness benchmarks for 2D images are created by changing the RGB values. Corruptions in the 3D space directly modify both the numbers and positions of points. The distributional shift is thus large between corrupted and clean point clouds.

• *Insight 4.2.* Test-time adaptation is surprisingly useful on tough corruptions.

We find that TENT on average helps achieve the strongest robustness on Occlusion (ER=47.6%), LiDAR (ER=54.1%), and Rotation (ER=19.8%) corruptions, outperforming the best augmentation method by 6.7%, 1.9%, and 7.9% respectively. Especially, we find test-time adaptation methods achieve the best ER_{rotation,5} = 35.6%, which is a 27.1% improvement over the best augmentation strategy. Augmentation strategies cannot handle these difficult corruptions, but test-time adaptation methods deliver a more consistent improvement.

Table 5. Error Rates of Different Model Architectures on ModelNet40-C with PointCutMix-R and TENT.

Corruption (%) ↓	PointNet	PointNet++	DGCNN	RSCNN	PCT	SimpleView
Density	24.8	21.8	24.7	<u>22.7</u>	22.8	23.5
Noise	15.7	9.5	<u>9.2</u>	10.7	9.0	9.7
Trans.	15.2	12.1	<u>10.4</u>	12.9	10.1	13.3
ER _{cor}	18.5	<u>14.5</u>	14.8	15.4	13.9	15.5

We have so far demonstrated that PointCutMix-R and TENT obtain the best among the training- and test-time methods, in terms of the overall ER_{cor}. We here evaluate the performance of the combination of PointCutMix-R and TENT as they do not conflict with each other. As presented in Table 5, we find that the combined solution further improves the corruption robustness by 14.7%. To our best knowledge, there is no test-time adaptation designs specific for point cloud learning, and we hope our study will shed light on future research on corruption robustness in this area.

6. Discussion and Conclusion

Through our systematic benchmarking and analysis, we found that the performance discrepancies of different point cloud recognition models across different corruptions are much larger than 2D architectures. This suggests future studies on a universal architecture design for 3D point cloud to be a worthwhile direction. In the future, we plan to extend our current benchmark to complex tasks like point cloud segmentation and object detection to facilitate future research on robustness in the 3D domain.

To conclude, we have presented ModelNet40-C, the first comprehensive benchmark for corruption robustness of point cloud recognition models. We have unveiled the massive performance degradation on our ModelNet40-C for six representative models. We also provided critical insights on how different architecture and data augmentation designs affect model robustness on different corruptions. For example, Transformer appears to be a promising architecture in improving robustness in 3D vision tasks. Our study on test-time adaptation in point cloud recognition shows its potential as a robustness strategy. We hope that our ModelNet40-C benchmark will benefit future research in developing robust 3D point cloud models.

References

- Adallah, H. B., Orteu, J.-J., Dolives, B., and Jovančević, I. 3d point cloud analysis for automatic inspection of aeronautical mechanical assemblies. In *Fourteenth International Conference on Quality Control by Artificial Vision*, volume 11172, pp. 111720U. International Society for Optics and Photonics, 2019.
- Bai, Y., Mei, J., Yuille, A., and Xie, C. Are transformers more robust than cnns? In *NeurIPS*, 2021.
- Bonatto, D., Rogge, S., Schenkel, A., Ercek, R., and Lafruit, G. Explorations for real-time point cloud rendering of natural scenes in virtual reality. In *2016 International Conference on 3D Imaging (IC3D)*, pp. 1–7. IEEE, 2016.
- Bulusu, S., Kailkhura, B., Li, B., Varshney, P. K., and Song, D. Anomalous example detection in deep learning: A survey. *IEEE Access*, 8:132330–132347, 2020.
- Calian, D. A., Stimberg, F., Wiles, O., Rebuffi, S.-A., Gyorgy, A., Mann, T., and Goyal, S. Defending against image corruptions through adversarial augmentations. *arXiv preprint arXiv:2104.01086*, 2021.
- Cao, C., Preda, M., and Zaharia, T. 3d point cloud compression: A survey. In *The 24th International Conference on 3D Web Technology*, pp. 1–9, 2019.
- Carlini, N., Athalye, A., Papernot, N., Brendel, W., Rauber, J., Tsipras, D., Goodfellow, I., Madry, A., and Kurakin, A. On evaluating adversarial robustness. *arXiv preprint arXiv:1902.06705*, 2019.
- Chang, A. X., Funkhouser, T., Guibas, L., Hanrahan, P., Huang, Q., Li, Z., Savarese, S., Savva, M., Song, S., Su, H., et al. Shapenet: An information-rich 3d model repository. *arXiv preprint arXiv:1512.03012*, 2015.
- Chen, Y., Hu, V. T., Gavves, E., Mensink, T., Mettes, P., Yang, P., and Snoek, C. G. Pointmixup: Augmentation for point clouds. In *Computer Vision—ECCV 2020: 16th European Conference, Glasgow, UK, August 23–28, 2020, Proceedings, Part III 16*, pp. 330–345. Springer, 2020.
- Cheng, Q., Sun, P., Yang, C., Yang, Y., and Liu, P. X. A morphing-based 3d point cloud reconstruction framework for medical image processing. *Computer methods and programs in biomedicine*, 193:105495, 2020.
- Croce, F. and Hein, M. Reliable evaluation of adversarial robustness with an ensemble of diverse parameter-free attacks. In *International conference on machine learning*, pp. 2206–2216. PMLR, 2020.
- Croce, F., Andriushchenko, M., Sehwag, V., DeBenedetti, E., Flammarion, N., Chiang, M., Mittal, P., and Hein, M. Robustbench: a standardized adversarial robustness benchmark. *arXiv preprint arXiv:2010.09670*, 2020.
- Cubuk, E. D., Zoph, B., Mane, D., Vasudevan, V., and Le, Q. V. Autoaugment: Learning augmentation policies from data. *arXiv preprint arXiv:1805.09501*, 2018.
- Dai, A., Chang, A. X., Savva, M., Halber, M., Funkhouser, T., and Nießner, M. Scannet: Richly-annotated 3d reconstructions of indoor scenes. In *Proc. Computer Vision and Pattern Recognition (CVPR)*, IEEE, 2017.
- DeVries, T. and Taylor, G. W. Improved regularization of convolutional neural networks with cutout. *arXiv preprint arXiv:1708.04552*, 2017.
- Dong, X., Chen, D., Zhou, H., Hua, G., Zhang, W., and Yu, N. Self-robust 3d point recognition via gather-vector guidance. In *2020 IEEE/CVF Conference on Computer Vision and Pattern Recognition (CVPR)*, pp. 11513–11521. IEEE, 2020.
- Dosovitskiy, A., Beyer, L., Kolesnikov, A., Weissenborn, D., Zhai, X., Unterthiner, T., Dehghani, M., Minderer, M., Heigold, G., Gelly, S., Uszkoreit, J., and Houlsby, N. An image is worth 16x16 words: Transformers for image recognition at scale. In *International Conference on Learning Representations*, 2021. URL <https://openreview.net/forum?id=YicbFdNTTy>.
- Forti, D. and Rozza, G. Efficient geometrical parametrisation techniques of interfaces for reduced-order modelling: application to fluid–structure interaction coupling problems. *International Journal of Computational Fluid Dynamics*, 28(3-4):158–169, 2014.
- Geiger, A., Lenz, P., and Urtasun, R. Are we ready for autonomous driving? the kitti vision benchmark suite. In *Conference on Computer Vision and Pattern Recognition (CVPR)*, 2012.
- Goyal, A., Law, H., Liu, B., Newell, A., and Deng, J. Revisiting point cloud shape classification with a simple and effective baseline. *arXiv preprint arXiv:2106.05304*, 2021.
- Guo, M.-H., Cai, J.-X., Liu, Z.-N., Mu, T.-J., Martin, R. R., and Hu, S.-M. Pct: Point cloud transformer. *Computational Visual Media*, 7(2):187–199, 2021.
- He, K., Zhang, X., Ren, S., and Sun, J. Deep residual learning for image recognition. In *Proceedings of the IEEE conference on computer vision and pattern recognition*, pp. 770–778, 2016.
- Hendrycks, D. and Dietterich, T. Benchmarking neural network robustness to common corruptions and perturbations. *arXiv preprint arXiv:1903.12261*, 2019.
- Hendrycks, D., Mu, N., Cubuk, E. D., Zoph, B., Gilmer, J., and Lakshminarayanan, B. Augmix: A simple data processing method to improve robustness and uncertainty. *arXiv preprint arXiv:1912.02781*, 2019.
- Hendrycks, D., Basart, S., Mu, N., Kadavath, S., Wang, F., Dorundo, E., Desai, R., Zhu, T., Parajuli, S., Guo, M., et al. The many faces of robustness: A critical analysis of out-of-distribution generalization. In *Proceedings of the IEEE/CVF International Conference on Computer Vision*, pp. 8340–8349, 2021.
- Ioffe, S. and Szegedy, C. Batch normalization: Accelerating deep network training by reducing internal covariate shift. In *International conference on machine learning*, pp. 448–456. PMLR, 2015.
- Kingma, D. P. and Ba, J. Adam: A method for stochastic optimization, 2014.
- Koh, P. W., Sagawa, S., Marklund, H., Xie, S. M., Zhang, M., Balsubramani, A., Hu, W., Yasunaga, M., Phillips, R. L., Gao, I., et al. Wilds: A benchmark of in-the-wild distribution shifts. In *International Conference on Machine Learning*, pp. 5637–5664. PMLR, 2021.

- Landrieu, L. and Simonovsky, M. Large-scale point cloud semantic segmentation with superpoint graphs. In *Proceedings of the IEEE conference on computer vision and pattern recognition*, pp. 4558–4567, 2018.
- Lee, D., Lee, J., Lee, J., Lee, H., Lee, M., Woo, S., and Lee, S. Regularization strategy for point cloud via rigidly mixed sample. In *Proceedings of the IEEE/CVF Conference on Computer Vision and Pattern Recognition*, pp. 15900–15909, 2021.
- Li, C.-L., Zaheer, M., Zhang, Y., Poczos, B., and Salakhutdinov, R. Point cloud gan. *arXiv preprint arXiv:1810.05795*, 2018a.
- Li, Y., Bu, R., Sun, M., Wu, W., Di, X., and Chen, B. Pointcnn: Convolution on x-transformed points. *Advances in neural information processing systems*, 31:820–830, 2018b.
- Liu, D., Yu, R., and Su, H. Extending adversarial attacks and defenses to deep 3d point cloud classifiers. In *2019 IEEE International Conference on Image Processing (ICIP)*, pp. 2279–2283. IEEE, 2019a.
- Liu, H., Jia, J., and Gong, N. Z. Pointguard: Provably robust 3d point cloud classification. In *Proceedings of the IEEE/CVF Conference on Computer Vision and Pattern Recognition*, pp. 6186–6195, 2021.
- Liu, J., Sun, Q., Fan, Z., and Jia, Y. Tof lidar development in autonomous vehicle. In *2018 IEEE 3rd Optoelectronics Global Conference (OGC)*, pp. 185–190. IEEE, 2018.
- Liu, Y., Fan, B., Xiang, S., and Pan, C. Relation-shape convolutional neural network for point cloud analysis. In *Proceedings of the IEEE/CVF Conference on Computer Vision and Pattern Recognition*, pp. 8895–8904, 2019b.
- Maloca, P. M., de Carvalho, J. E. R., Heeren, T., Hasler, P. W., Mushtaq, F., Mon-Williams, M., Scholl, H. P., Balaskas, K., Egan, C., Tufail, A., et al. High-performance virtual reality volume rendering of original optical coherence tomography point-cloud data enhanced with real-time ray casting. *Translational vision science & technology*, 7(4):2–2, 2018.
- Maturana, D. and Scherer, S. Voxnet: A 3d convolutional neural network for real-time object recognition. In *2015 IEEE/RSJ International Conference on Intelligent Robots and Systems (IROS)*, pp. 922–928. IEEE, 2015.
- Michaelis, C., Mitzkus, B., Geirhos, R., Rusak, E., Bringmann, O., Ecker, A. S., Bethge, M., and Brendel, W. Benchmarking robustness in object detection: Autonomous driving when winter is coming. *arXiv preprint arXiv:1907.07484*, 2019.
- Mintun, E., Kirillov, A., and Xie, S. On interaction between augmentations and corruptions in natural corruption robustness. *arXiv preprint arXiv:2102.11273*, 2021.
- Nguyen, A. and Le, B. 3d point cloud segmentation: A survey. In *2013 6th IEEE conference on robotics, automation and mechatronics (RAM)*, pp. 225–230. IEEE, 2013.
- Paszke, A., Gross, S., Massa, F., Lerer, A., Bradbury, J., Chanan, G., Killeen, T., Lin, Z., Gimelshein, N., Antiga, L., et al. Pytorch: An imperative style, high-performance deep learning library. *Advances in neural information processing systems*, 32: 8026–8037, 2019.
- Pomerleau, F., Colas, F., and Siegwart, R. A review of point cloud registration algorithms for mobile robotics. *Foundations and Trends in Robotics*, 4(1):1–104, 2015.
- Qi, C. R., Su, H., Mo, K., and Guibas, L. J. Pointnet: Deep learning on point sets for 3d classification and segmentation. In *Proceedings of the IEEE conference on computer vision and pattern recognition*, pp. 652–660, 2017a.
- Qi, C. R., Yi, L., Su, H., and Guibas, L. J. Pointnet++: Deep hierarchical feature learning on point sets in a metric space. *arXiv preprint arXiv:1706.02413*, 2017b.
- Roth, A. E. *The Shapley value: essays in honor of Lloyd S. Shapley*. Cambridge University Press, 1988.
- Schneider, S., Rusak, E., Eck, L., Bringmann, O., Brendel, W., and Bethge, M. Improving robustness against common corruptions by covariate shift adaptation. *arXiv preprint arXiv:2006.16971*, 2020.
- Sederberg, T. W. and Parry, S. R. Free-form deformation of solid geometric models. In *Proceedings of the 13th annual conference on Computer graphics and interactive techniques*, pp. 151–160, 1986.
- Shen, W., Ren, Q., Liu, D., and Zhang, Q. Interpreting representation quality of dnns for 3d point cloud processing. *Advances in Neural Information Processing Systems*, 34, 2021a.
- Shen, W., Wei, Z., Huang, S., Zhang, B., Chen, P., Zhao, P., and Zhang, Q. Verifiability and predictability: Interpreting utilities of network architectures for point cloud processing. In *Proceedings of the IEEE/CVF Conference on Computer Vision and Pattern Recognition (CVPR)*, pp. 10703–10712, June 2021b.
- Shen, Y., Feng, C., Yang, Y., and Tian, D. Mining point cloud local structures by kernel correlation and graph pooling. In *Proceedings of the IEEE conference on computer vision and pattern recognition*, pp. 4548–4557, 2018.
- Shi, S., Wang, X., and Li, H. Pointcnn: 3d object proposal generation and detection from point cloud. In *Proceedings of the IEEE/CVF conference on computer vision and pattern recognition*, pp. 770–779, 2019.
- Shi, S., Guo, C., Jiang, L., Wang, Z., Shi, J., Wang, X., and Li, H. Pv-rcnn: Point-voxel feature set abstraction for 3d object detection. In *Proceedings of the IEEE/CVF Conference on Computer Vision and Pattern Recognition*, pp. 10529–10538, 2020.
- Sun, J., Cao, Y., Chen, Q. A., and Mao, Z. M. Towards robust lidar-based perception in autonomous driving: General black-box adversarial sensor attack and countermeasures. In *29th {USENIX} Security Symposium ({USENIX} Security 20)*, pp. 877–894, 2020a.
- Sun, J., Koenig, K., Cao, Y., Chen, Q. A., and Mao, Z. M. On adversarial robustness of 3d point cloud classification under adaptive attacks. *arXiv preprint arXiv:2011.11922*, 2020b.
- Sun, J., Cao, Y., Choy, C. B., Yu, Z., Anandkumar, A., Mao, Z. M., and Xiao, C. Adversarially robust 3d point cloud recognition using self-supervisions. *Advances in Neural Information Processing Systems*, 34, 2021a.

- Sun, J., Mehra, A., Kailkhura, B., Chen, P.-Y., Hendrycks, D., Hamm, J., and Mao, Z. M. Certified adversarial defenses meet out-of-distribution corruptions: Benchmarking robustness and simple baselines. *arXiv preprint arXiv:2112.00659*, 2021b.
- Thomas, H., Qi, C. R., Deschaud, J.-E., Marcotegui, B., Goulette, F., and Guibas, L. J. Kpconv: Flexible and deformable convolution for point clouds. In *Proceedings of the IEEE/CVF International Conference on Computer Vision*, pp. 6411–6420, 2019.
- Uy, M. A., Pham, Q.-H., Hua, B.-S., Nguyen, T., and Yeung, S.-K. Revisiting point cloud classification: A new benchmark dataset and classification model on real-world data. In *Proceedings of the IEEE/CVF International Conference on Computer Vision*, pp. 1588–1597, 2019.
- Vaswani, A., Shazeer, N., Parmar, N., Uszkoreit, J., Jones, L., Gomez, A. N., Kaiser, L. u., and Polosukhin, I. Attention is all you need. In Guyon, I., Luxburg, U. V., Bengio, S., Wallach, H., Fergus, R., Vishwanathan, S., and Garnett, R. (eds.), *Advances in Neural Information Processing Systems*, volume 30. Curran Associates, Inc., 2017. URL <https://proceedings.neurips.cc/paper/2017/file/3f5ee243547dee91fbd053c1c4a845aa-Paper.pdf>.
- Wang, D., Shelhamer, E., Liu, S., Olshausen, B., and Darrell, T. Tent: Fully test-time adaptation by entropy minimization. *arXiv preprint arXiv:2006.10726*, 2020.
- Wang, D. Z. and Posner, I. Voting for voting in online point cloud object detection. In *Robotics: Science and Systems*, volume 1, pp. 10–15607. Rome, Italy, 2015.
- Wang, Y. and Solomon, J. M. Deep closest point: Learning representations for point cloud registration. In *Proceedings of the IEEE/CVF International Conference on Computer Vision*, pp. 3523–3532, 2019.
- Wang, Y., Sun, Y., Liu, Z., Sarma, S. E., Bronstein, M. M., and Solomon, J. M. Dynamic graph cnn for learning on point clouds. *Acm Transactions On Graphics (tog)*, 38(5):1–12, 2019.
- Wolff, K., Kim, C., Zimmer, H., Schroers, C., Botsch, M., Sorkine-Hornung, O., and Sorkine-Hornung, A. Point cloud noise and outlier removal for image-based 3d reconstruction. In *2016 Fourth International Conference on 3D Vision (3DV)*, pp. 118–127. IEEE, 2016.
- Wu, W., Qi, Z., and Fuxin, L. Pointconv: Deep convolutional networks on 3d point clouds. In *Proceedings of the IEEE/CVF Conference on Computer Vision and Pattern Recognition*, pp. 9621–9630, 2019.
- Wu, Z., Song, S., Khosla, A., Yu, F., Zhang, L., Tang, X., and Xiao, J. 3d shapenets: A deep representation for volumetric shapes. In *Proceedings of the IEEE conference on computer vision and pattern recognition*, pp. 1912–1920, 2015.
- Xiang, C., Qi, C. R., and Li, B. Generating 3d adversarial point clouds. In *Proceedings of the IEEE/CVF Conference on Computer Vision and Pattern Recognition*, pp. 9136–9144, 2019.
- Yang, W., Gong, Z., Huang, B., and Hong, X. Lidar with velocity: Motion distortion correction of point clouds from oscillating scanning lidars. *arXiv preprint arXiv:2111.09497*, 2021.
- Yin, T., Zhou, X., and Krahenbuhl, P. Center-based 3d object detection and tracking. In *Proceedings of the IEEE/CVF Conference on Computer Vision and Pattern Recognition*, pp. 11784–11793, 2021.
- Yu, J., Zhang, C., Wang, H., Zhang, D., Song, Y., Xiang, T., Liu, D., and Cai, W. 3d medical point transformer: Introducing convolution to attention networks for medical point cloud analysis. *arXiv preprint arXiv:2112.04863*, 2021.
- Zhang, J., Chen, L., Ouyang, B., Liu, B., Zhu, J., Chen, Y., Meng, Y., and Wu, D. Pointcutmix: Regularization strategy for point cloud classification. *arXiv preprint arXiv:2101.01461*, 2021.
- Zhao, H., Jiang, L., Jia, J., Torr, P. H., and Koltun, V. Point transformer. In *Proceedings of the IEEE/CVF International Conference on Computer Vision*, pp. 16259–16268, 2021.
- Zhao, Y., Wu, Y., Chen, C., and Lim, A. On isometry robustness of deep 3d point cloud models under adversarial attacks. In *Proceedings of the IEEE/CVF Conference on Computer Vision and Pattern Recognition*, pp. 1201–1210, 2020.
- Zhou, H., Chen, K., Zhang, W., Fang, H., Zhou, W., and Yu, N. Dup-net: Denoiser and upsampler network for 3d adversarial point clouds defense. In *Proceedings of the IEEE/CVF International Conference on Computer Vision*, pp. 1961–1970, 2019.
- Zhou, L., Du, Y., and Wu, J. 3d shape generation and completion through point-voxel diffusion. *arXiv preprint arXiv:2104.03670*, 2021.
- Zhou, Q.-Y., Park, J., and Koltun, V. Open3D: A modern library for 3D data processing. *arXiv:1801.09847*, 2018.

A. ModelNet40-C

We elaborate the creation of ModelNet40-C in this section. The detailed implementation can be found in our codebase, which is included in the supplementary materials.

`Occlusion` and `LiDAR` share similar general corruption features. We leverage five viewing angles to construct these two corruptions on ModelNet40, as shown in Fig. A. Specifically, we utilize ray tracing algorithms on the original meshed from ModelNet40 to generate the point cloud. Let the facing direction of the object as 0° pivoting the z axis, we use 0° , 72° , 144° , 216° , and 288° as our viewing angles, the viewing angles between the xy plane are randomly sampled from is $30^\circ - 60^\circ$. For `LiDAR`, we additionally render the generated point cloud into the vertically multi-line style to simulate the pattern of the LiDAR sensor.

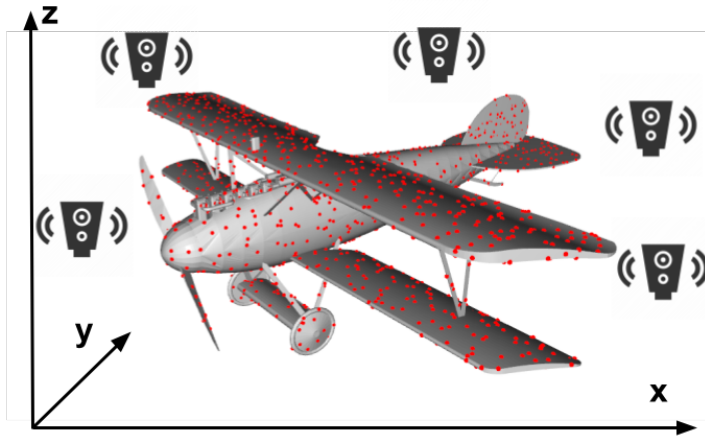


Figure 5. Illustration of `Occlusion` and `LiDAR` Corruption Generation.

For `LocalDensityInc` and `LocalDensityDec`, we first sample a number of anchor points based the severity level. We further find the k NN of the anchor points and up-sample or down-sample them to increase and decrease their local density, respectively. Similarly, `Cutout` discards the full k NN ($k = 50$) subsets of the anchor points to simulate the sensor limitations of LiDAR and other scanning devices.

`Gaussian` and `Uniform` noises are sampled from Gaussian and uniform distributions with different σ and ϵ based on the severity level. For the `Background` noise, we randomly sample different numbers of points in the edge-length-2 cube that bounds the point cloud based on the severity level. For `Impulse` noise, we first sample different numbers of points based on the severity level and assign the maximum magnitude of perturbation $\ell_\infty = 0.05$ to them. For the `Upsampling` noise, we first choose different numbers of points based on the severity level and generate new points around the selected anchors, bounded by $\ell_\infty = 0.05$.

For `Rotation` and `Shear`, we have introduced their construction in § 3. As mentioned, we allow relatively small transformations since we find larger ones will affect the human perception of the object class as well.

For deformation-based corruptions `FFD`, `RBF`, and `Inv_RBF`, we assign 5 control points along each xyz axis, resulting in 125 control points in total. We choose the deformation distance based on the severity level and randomly assign their directions in the 3D space. The deformations then are formulated based on the interpolation functions that we choose in § 3.

We visualize two additional groups of sample point clouds from ModelNet40-C in Fig. 6. and 7.

B. Experiments

B.1. Data Augmentation Setups

We introduce the detailed setting of our experiments and analysis in this section. For all mixing-based data augmentation strategies, we have a hyper-parameter λ to determine the weight of two samples to mix, as well as the weight of the virtual label vector:

$$y_{aug} = \lambda \cdot y_a + (1 - \lambda) \cdot y_b \quad (1)$$

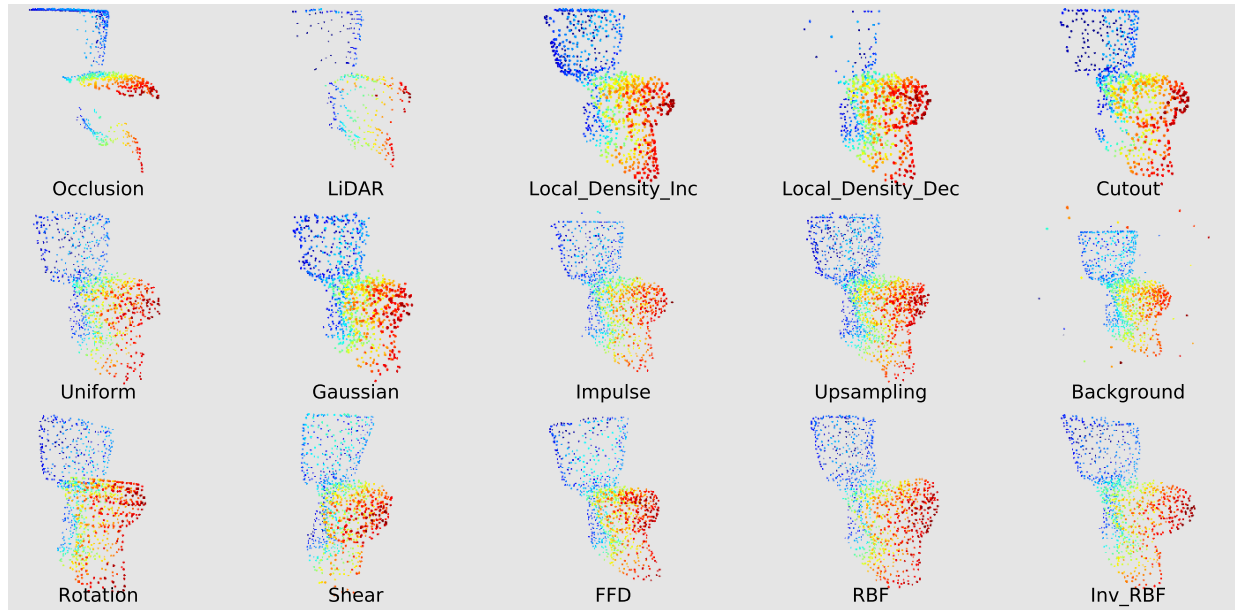


Figure 6. Visualization of Samples from ModelNet40-C - “Toilet” Class.

where y_a and y_b are the label vectors for point cloud x_a and x_b . We set $\lambda = 0.5$, which has shown to achieve good results reported in (Zhang et al., 2021; Chen et al., 2020; Lee et al., 2021). For adversarial training, we use the point shifting attack in the adversarial inner maximization:

$$\mathbf{x}^{s+1} = \Pi_{\mathbf{x}+\mathcal{S}}(\mathbf{x}^s + \alpha \cdot \text{sign}(\nabla_{\mathbf{x}^s} \mathcal{L}(\mathbf{x}^s, y; f))); \quad \mathbf{x}^0 = \mathbf{x} + \text{U}(-\epsilon, \epsilon) \quad (2)$$

where $\epsilon = 0.05$, $\alpha = 0.01$ and we use seven steps PGD, as suggested by Sun et al. (2021a).

B.2. Evaluation Results

We illustrate the confusion matrices of all six models with standard training in Fig. 8 to show the validity of ModelNet40-C. We present our detailed evaluation results containing 3,180 data points. Fig. 9 and 10 shows the model comparison on all data augmentation strategies. The class-wise mean error rates (mER) are shown in Figure 11 and 12. The detailed results of test-time adaptation methods (ER and mER) are shown in Fig. 13, 14, 15, and 16.

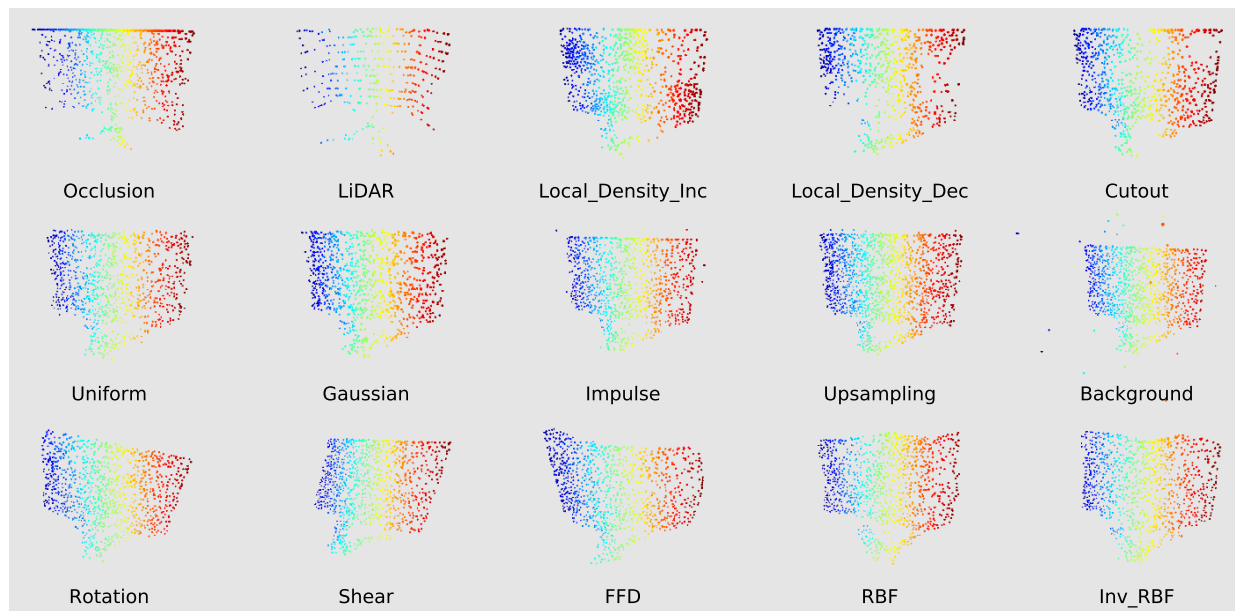


Figure 7. Visualization of Samples from ModelNet40-C - "Monitor" Class.

Benchmarking Robustness of 3D Point Cloud Recognition Against Common Corruptions

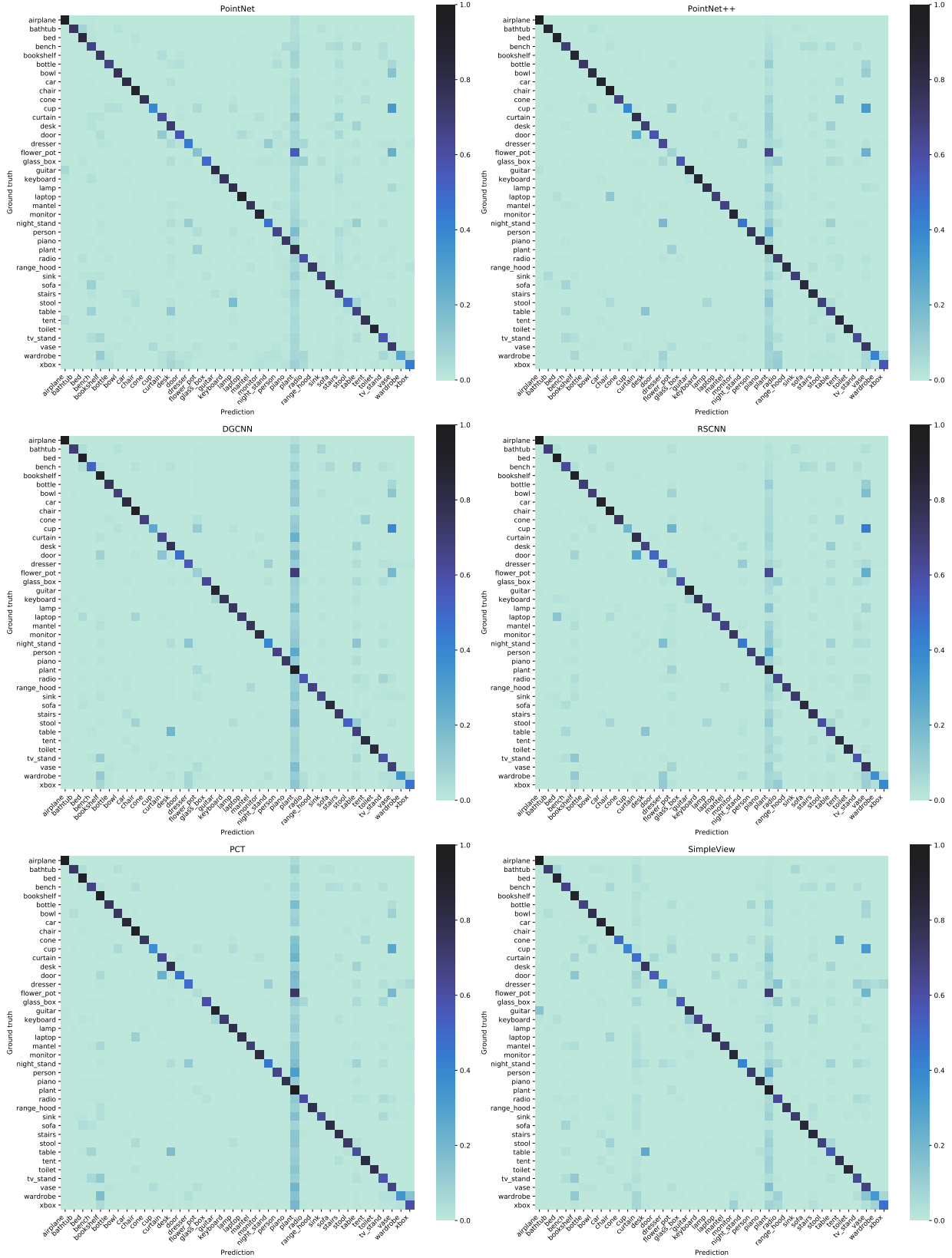


Figure 8. Confusion Matrices for Each Model on ModelNet40-C with Standard Training.

Benchmarking Robustness of 3D Point Cloud Recognition Against Common Corruptions

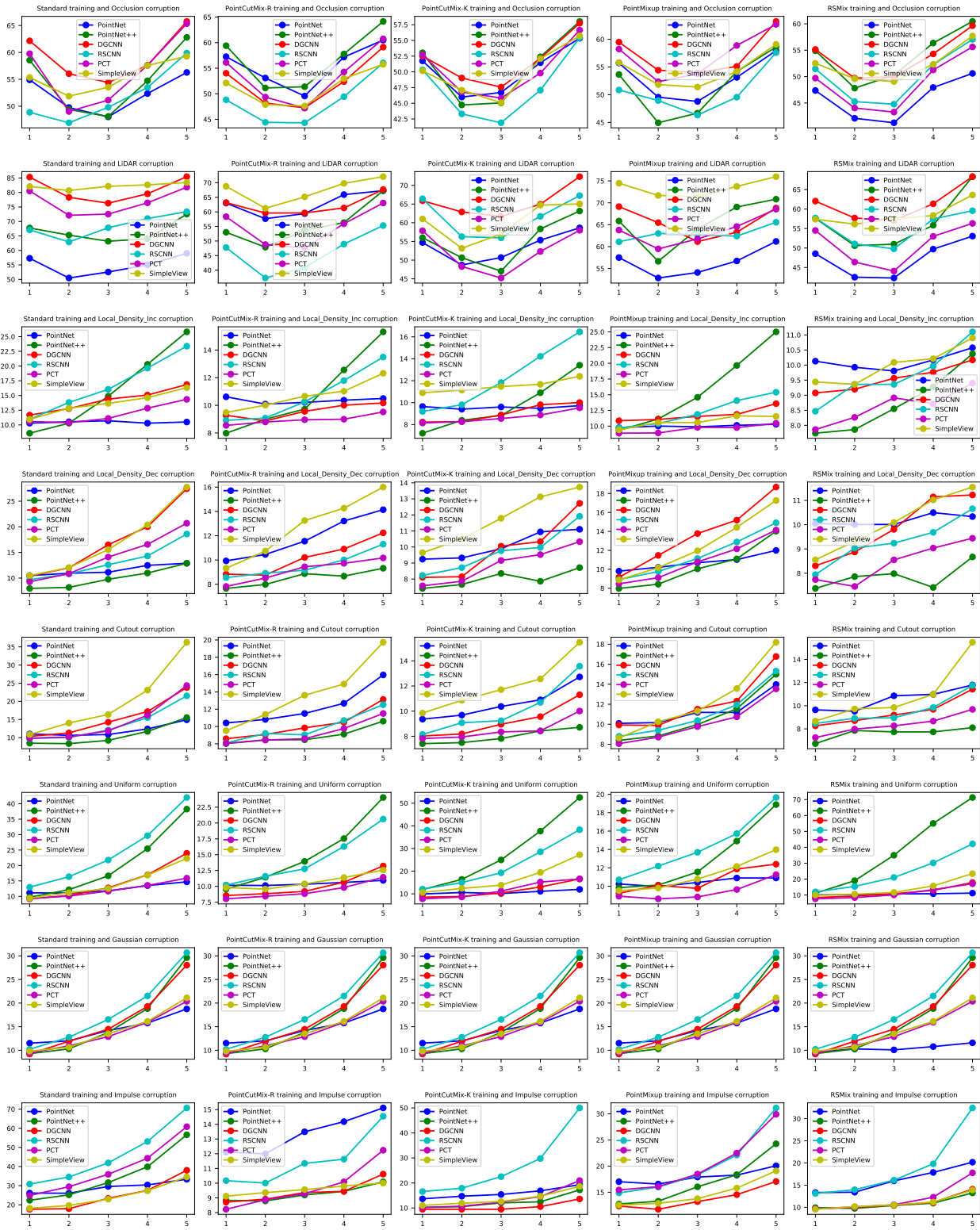


Figure 9. Error Rates of Different Models with Different Data Augmentation Strategies on ModelNet40-C.

Benchmarking Robustness of 3D Point Cloud Recognition Against Common Corruptions

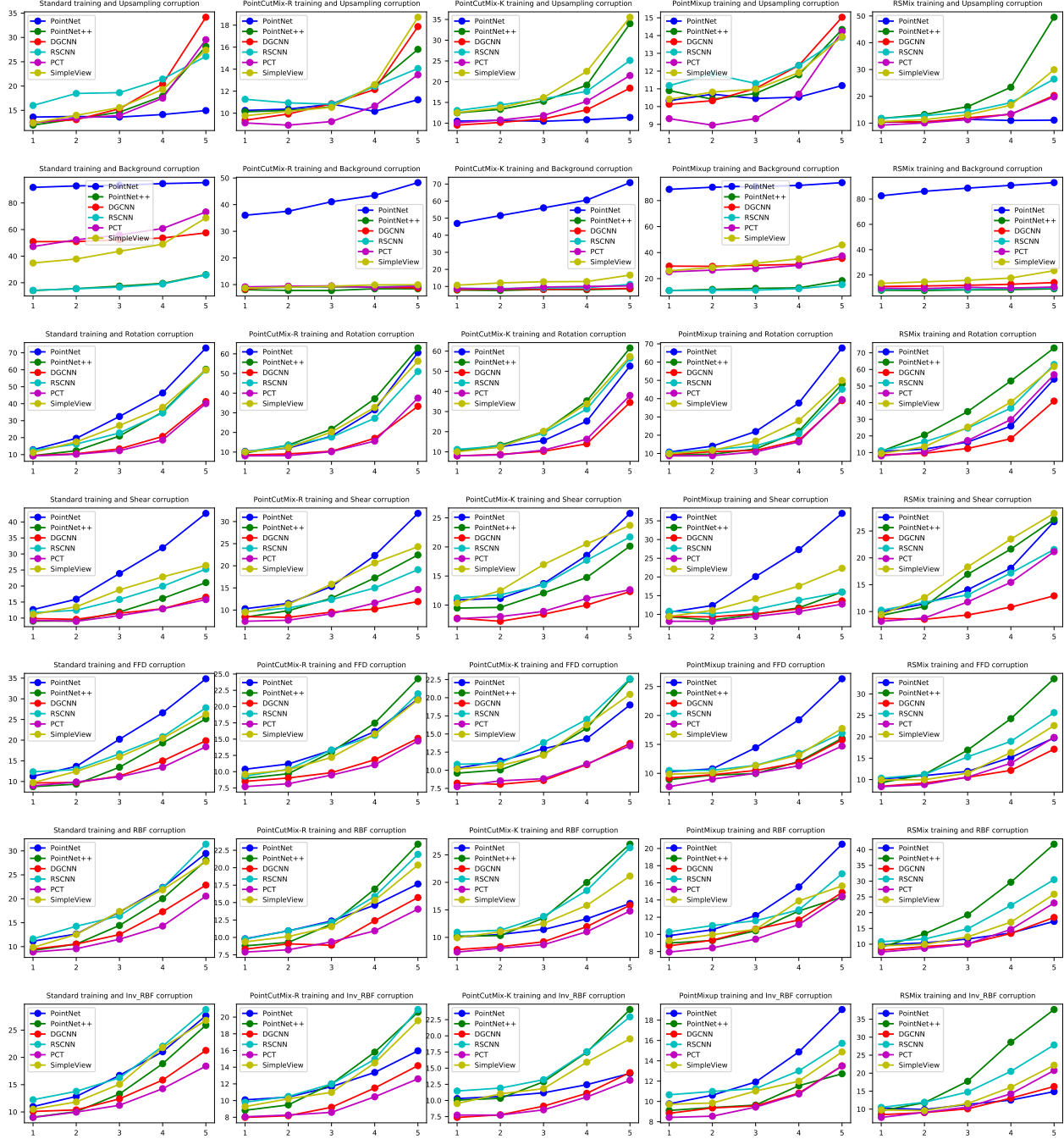


Figure 10. Error Rates of Different Models with Different Data Augmentation Strategies on ModelNet40-C (Cont'd).

Benchmarking Robustness of 3D Point Cloud Recognition Against Common Corruptions

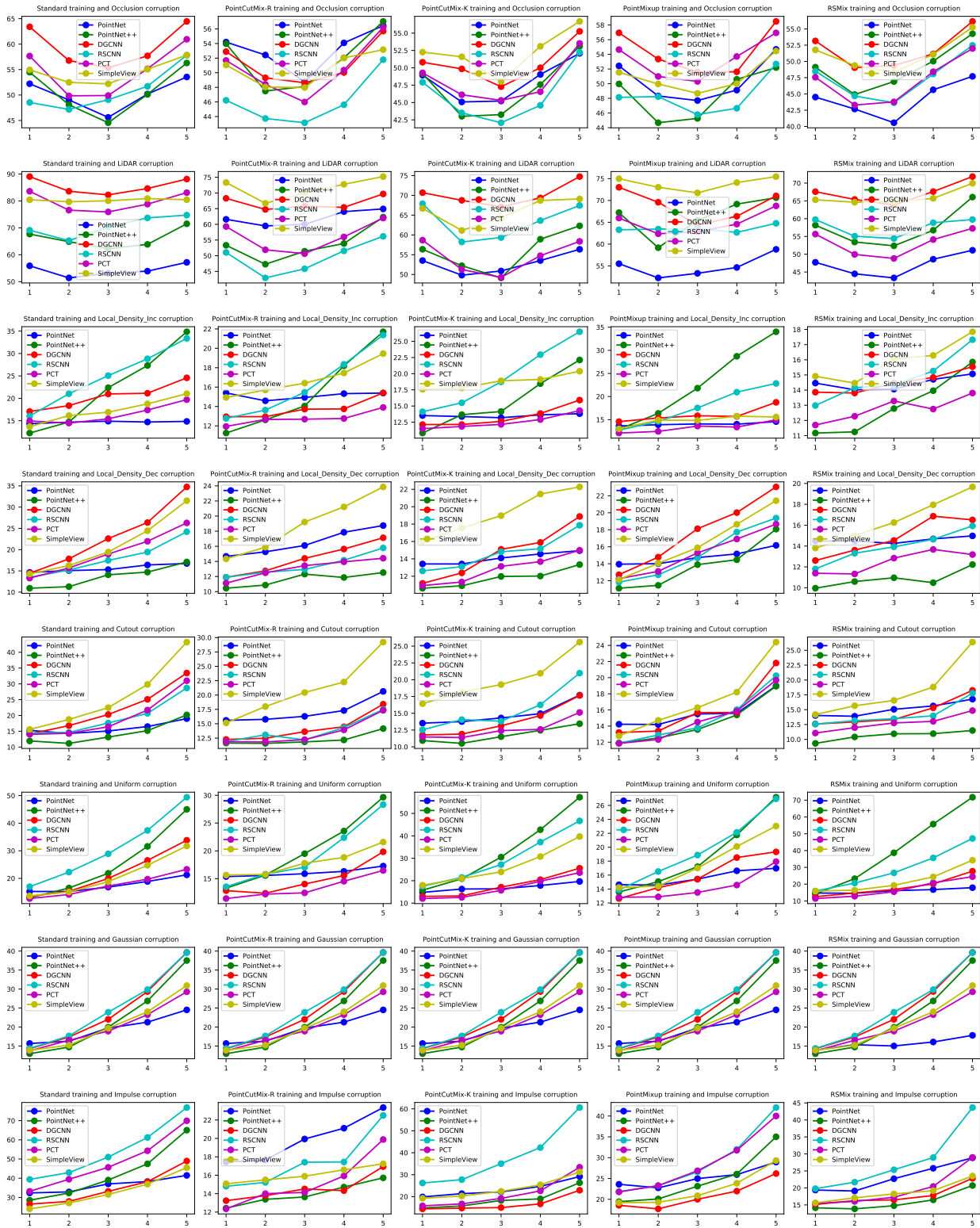


Figure 11. Class-wise Mean Error Rates of Different Models with Different Data Augmentation Strategies on ModelNet40-C.

Benchmarking Robustness of 3D Point Cloud Recognition Against Common Corruptions

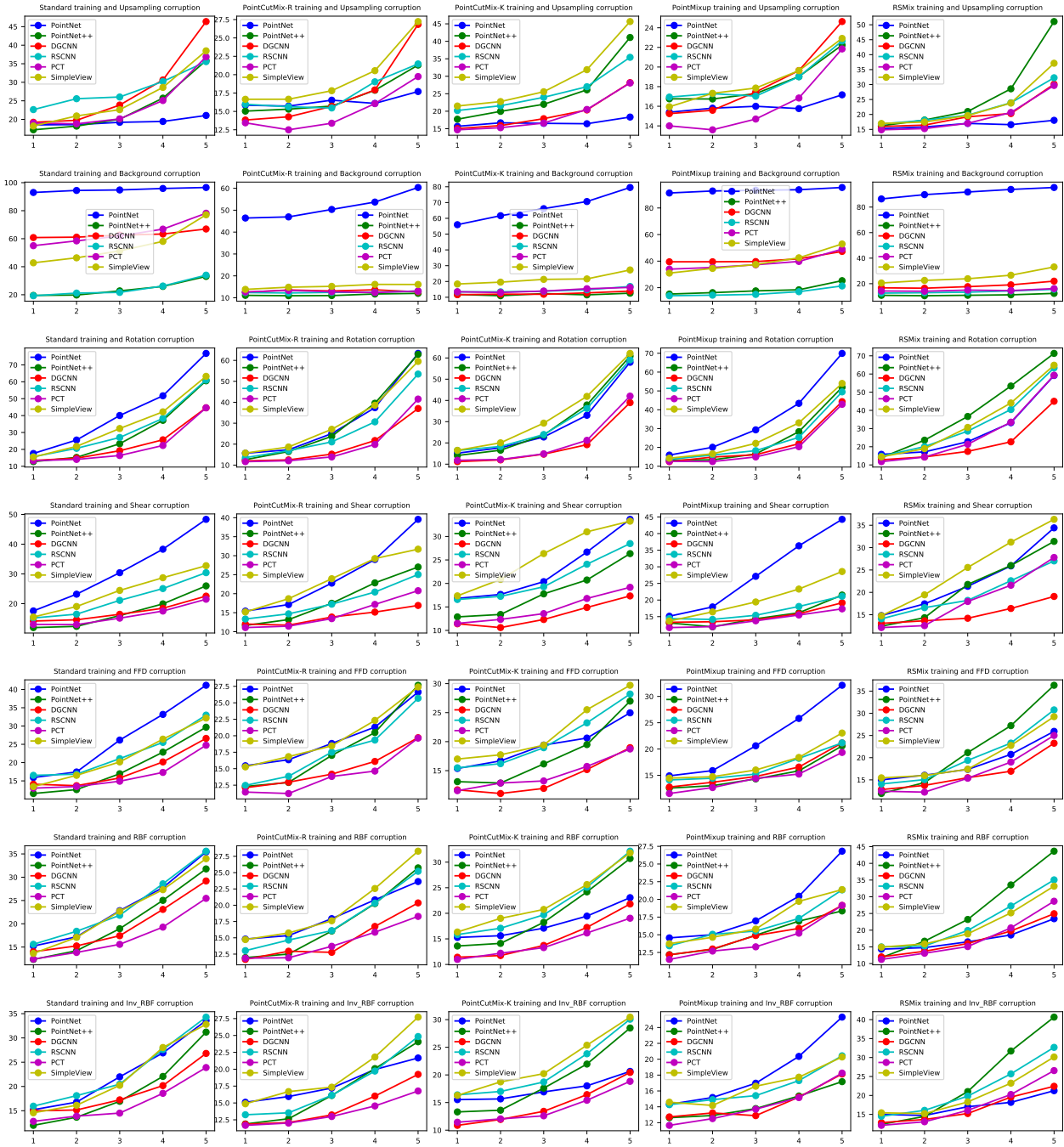


Figure 12. Class-wise Mean Error Rates of Different Models with Different Data Augmentation Strategies on ModelNet40-C (Cont'd).

Benchmarking Robustness of 3D Point Cloud Recognition Against Common Corruptions

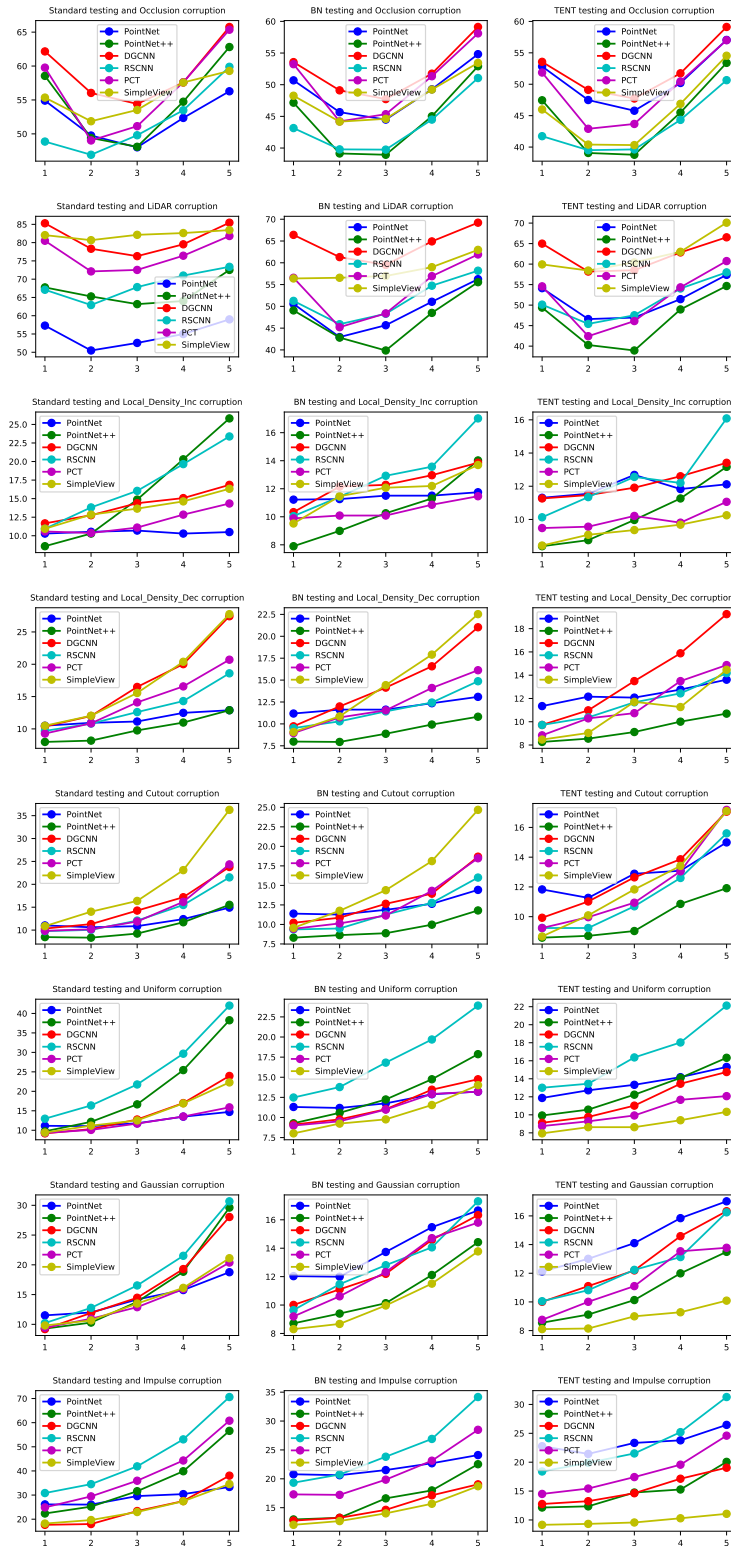


Figure 13. Error Rates of Different Models with Different Test-time Adaptation Methods on ModelNet40-C.

Benchmarking Robustness of 3D Point Cloud Recognition Against Common Corruptions

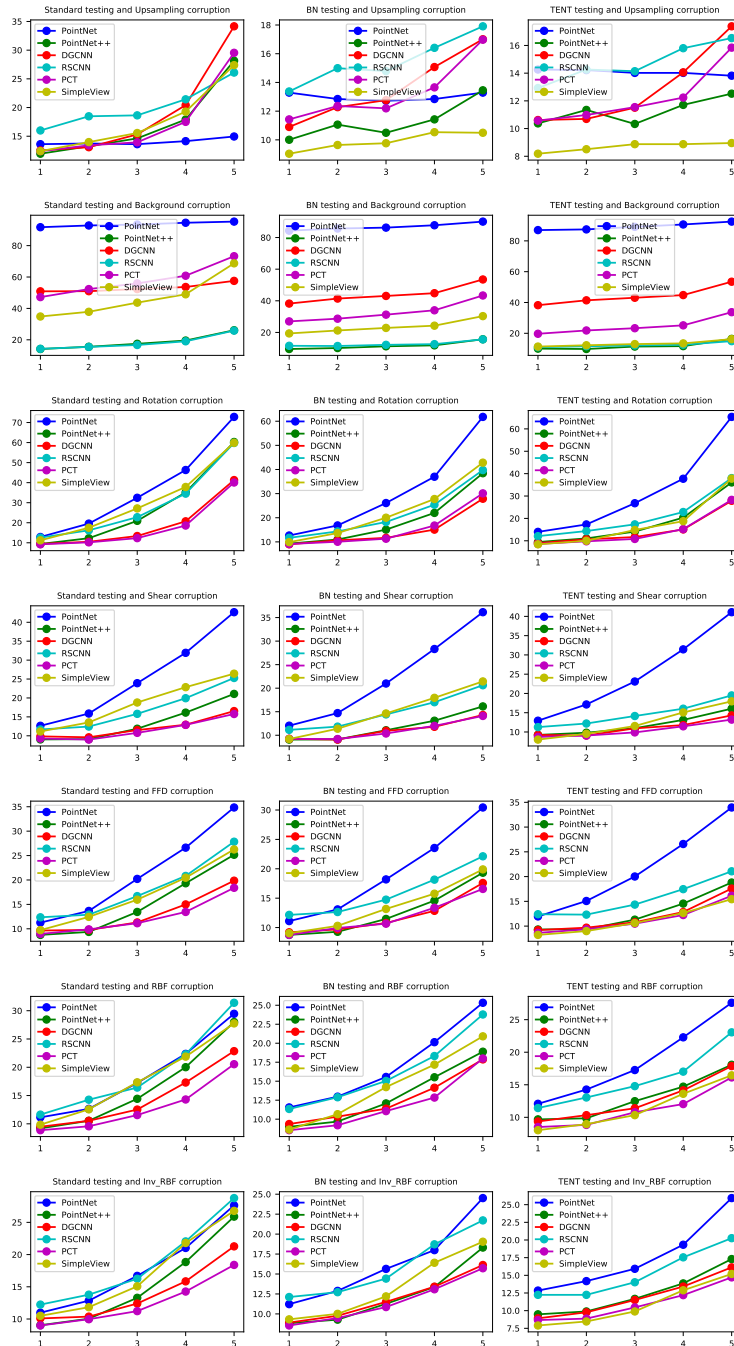


Figure 14. Error Rates of Different Models with Different Test-time Adaptation Methods on ModelNet40-C (Cont'd).

Benchmarking Robustness of 3D Point Cloud Recognition Against Common Corruptions

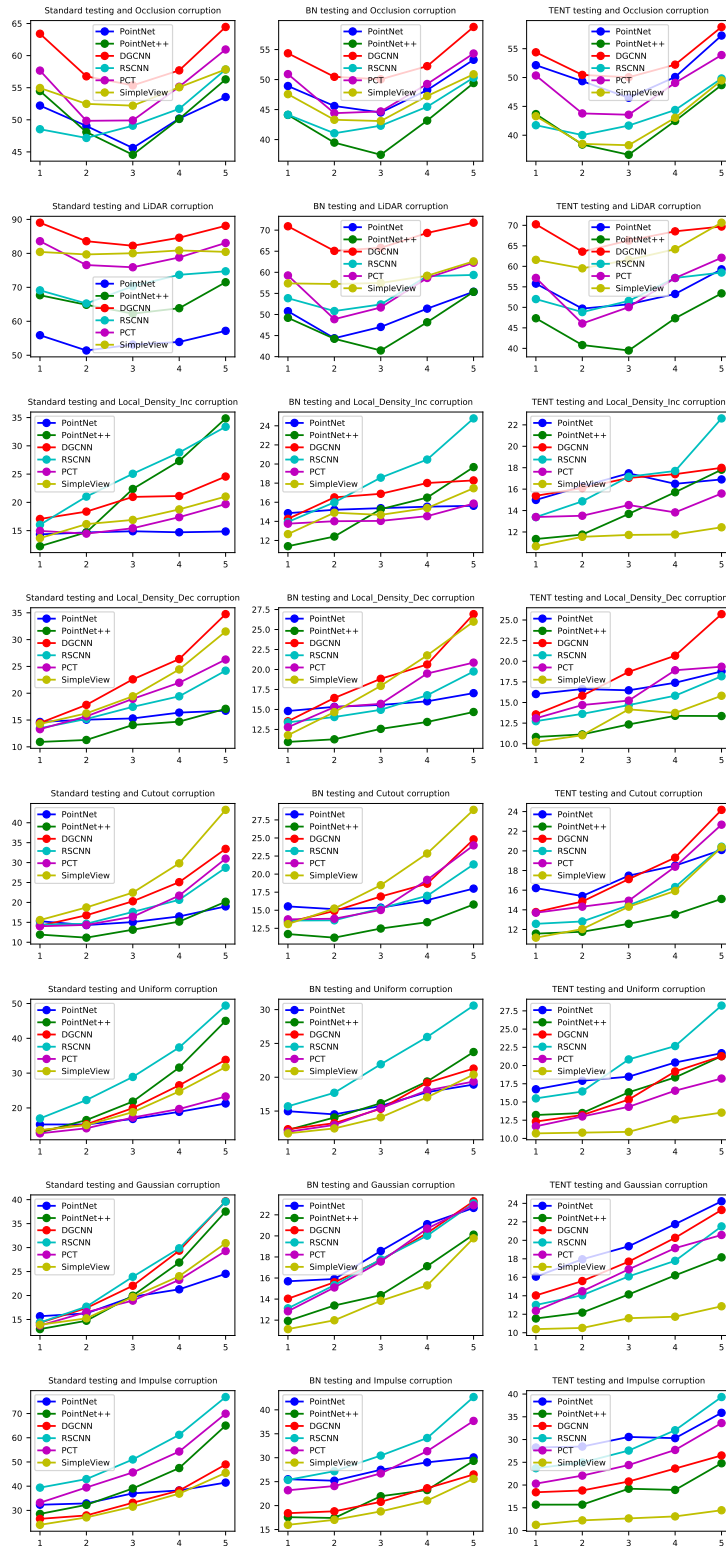


Figure 15. Class-wise Mean Error Rates of Different Models with Different Test-time Adaptation Methods on ModelNet40-C.

Benchmarking Robustness of 3D Point Cloud Recognition Against Common Corruptions

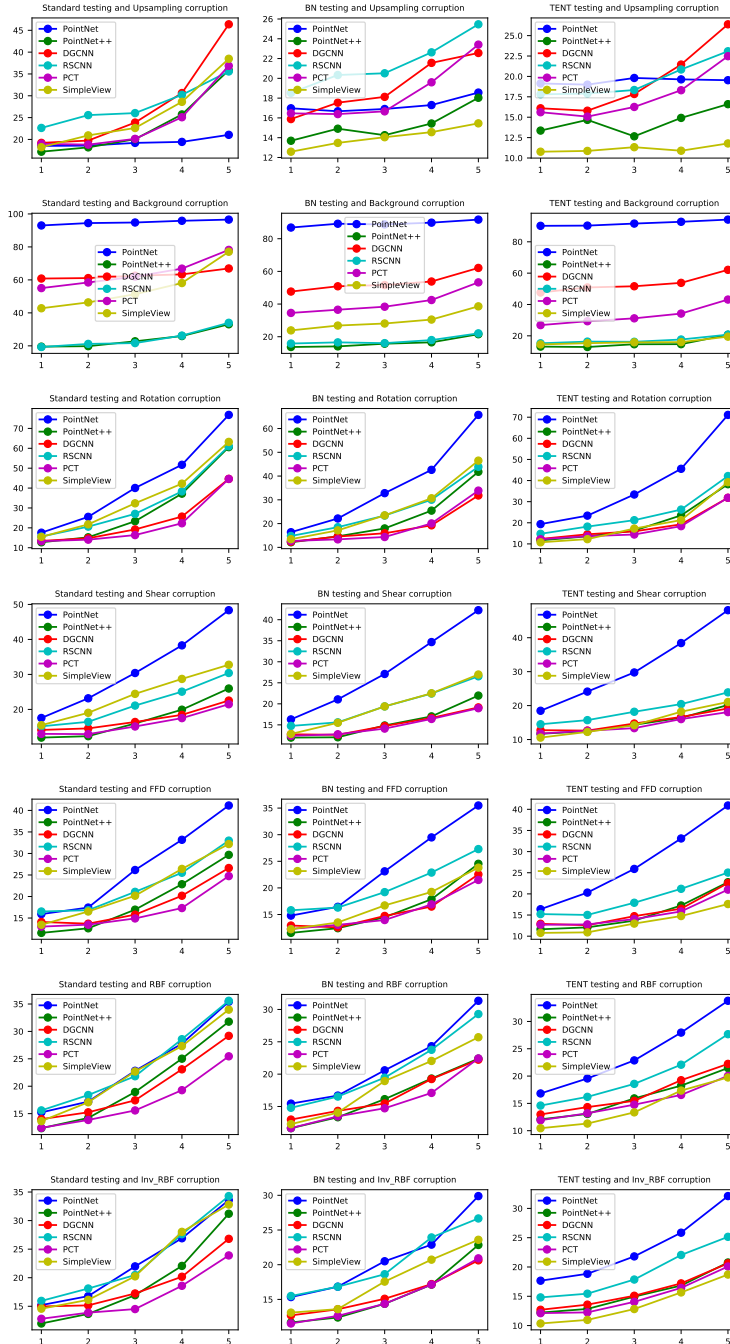


Figure 16. Class-wise Mean Error Rates of Different Models with Different Test-time Adaptation Methods on ModelNet40-C (Cont'd).